

Comparing the Vertical Structures of Weighting Functions and Adjoint Sensitivity of Radiance and Verifying Mesoscale Forecasts Using AIRS Radiance Observations

MATTHEW J. CARRIER AND XIAOLEI ZOU

The Florida State University, Tallahassee, Florida

WILLIAM M. LAPENTA

Global Hydrology and Climate Center, NASA Marshall Space Flight Center, Huntsville, Alabama

(Manuscript received 19 October 2006, in final form 17 May 2007)

ABSTRACT

An adjoint sensitivity analysis is conducted using the adjoint of the hyperspectral radiative transfer model (RTM) that simulates the radiance spectrum from the Advanced Infrared Sounder (AIRS). It is shown, both theoretically and numerically, that the height of the maximum sensitivity of radiance in a channel could be higher or lower than the height of the maximum weighting function of that channel. It is shown that the discrepancy between the two heights is determined by the vertical structures of the atmospheric thermodynamic state. The sensitivity finds the level at which changes in temperature and/or moisture will have the largest influence on the simulated brightness temperature (BT), and the maximum weighting function (WF) height indicates the level where the model atmosphere contributes most significantly to the emission at the top of the atmosphere. Based on the above findings, an adjoint method for forecast verification using AIRS radiances is presented. In this method, model forecasts are first mapped into radiance space by an RTM so that they can be compared directly with the observed radiance values. The adjoint sensitivity analysis results are then used to connect the deviations of the model forecasts from observed radiances to the changes of temperature and moisture variables in model space. This adjoint sensitivity based model verification provides useful information on forecast model performances based on indirect observations from satellites.

1. Introduction

Atmospheric infrared soundings from orbiting satellites can provide valuable information regarding numerous meteorological parameters including atmospheric temperature and moisture profiles. Data from numerous satellite sounders, including the High Resolution Infrared Radiation Sounder (HIRS) and the Advanced Microwave Sounding Unit (AMSU), have led to advances in weather forecasting (Derber and Wu 1998; Baker et al. 2005) by utilizing the data through assimilation. However, whereas HIRS scans 20 spectral channels, and AMSU collects data from 16 microwave channels, the Atmospheric Infrared Sounder (AIRS) carried on board NASA's *Aqua* satellite is able to simultaneously scan 2378 spectral channels (Pagano et al.

2002), affording very high vertical resolution in AIRS atmospheric retrievals (Chahine et al. 2001). AIRS data have already led to improvements in weather forecasting (McNally et al. 2006; Le Marshall et al. 2006) by directly assimilating AIRS radiances. Another application of AIRS data that takes advantage of its high spectral resolution is the direct use of AIRS radiance observations at different channels for mesoscale forecast verification, which is presented in this study.

Comparisons between simulated radiances and observed values are routinely done at various operational centers prior to assimilating the radiance data into their respective forecast models (McNally et al. 2006; Le Marshall et al. 2006). This is done for several reasons: 1) to ensure that simulated radiances do not deviate significantly from the observations to be assimilated in a data assimilation system (a quality control procedure done prior to data assimilation), 2) to ensure that values of observational data are reasonable, 3) to monitor errors in the background analysis fields, and 4) to diagnose biases in the radiative transfer model, observa-

Corresponding author address: Matthew J. Carrier, Dept. of Meteorology, The Florida State University, 404 Love Bldg., Tallahassee, FL 32306.
E-mail: mcarrier@met.fsu.edu

tions, and background analysis. In this paper, an adjoint sensitivity method for forecast verification using AIRS radiances is presented. The deviations of the simulated radiances from observed radiances are used directly to infer which background model variable at what vertical level might have contributed most to the departures in the radiances.

To conduct this model verification, multiple tools need to be in place. First, to compare model forecasts directly with AIRS radiances, a radiative transfer model (RTM) must be used to map the forecasted model variables to radiance space. Second, a method must be devised to link errors in the radiance space back to the aforementioned forecast model variable space. Initially, one could use a priori information regarding the type of channel (carbon dioxide or water vapor channel) and channel-specific weighting functions (WFs) to link the simulated BT error back to the forecast model. This is, however, not the best choice for a model verification study. The WF only gives information as to the relative contribution of each RTM level to the emission at the top of the atmosphere for each channel. It does not provide information about the sensitivity of the BT calculation to changes in model variables (i.e., temperature or moisture) at different vertical levels. For studies requiring a linkage between output-variable perturbations to input-variable perturbations of a model operator (e.g., RTM in this case), it is best to use the sensitivity results.

A sensitivity analysis allows one to quantify the impact that certain atmospheric variables have on a selected model response, which for this study is radiance, or brightness temperature (BT). Traditional methods derive the sensitivity of modeled radiance at a specified channel by varying each of the input variables one at a time. Not only is accuracy a concern in this forward formulation of sensitivity, it is also highly inefficient when dealing with the numerous channels afforded by AIRS. A more efficient and accurate method for studying sensitivity is the so-called adjoint method. The adjoint sensitivity analysis requires the adjoint of the radiative transfer model, which allows simultaneous calculation of the radiance's sensitivity, at each channel, to all input variables with only one run of the forward RTM and one run of the adjoint RTM.

Adjoint sensitivity analysis has been conducted to study the sensitivities of model forecasts to initial conditions and/or physical parameters (Zou et al. 1993; Zupanski 1995; Gelaro et al. 1998). In this study, the relative sensitivity of satellite radiances to temperature and moisture at different vertical levels (Amerault and Zou 2003) is investigated for a hyperspectral sounder, that is, AIRS. For the sensitivity study of AIRS data, a

visualization of the sensitivity results is demonstrated that enables one to account for the thousands of channels in an efficient manner. In addition to this, a comparison study is done that illustrates and provides a rationale for the differences in the vertical structures of the sensitivity and the WFs determined by radiative transmittances. This study outlines the basis of using the sensitivity to provide the link between BT errors to errors in model variables of a mesoscale forecast.

The following paper is constructed as follows: in section 2 the selected RTM and its adjoint are introduced, and an overview of the AIRS data and the selected test case are presented. Section 3 highlights the mathematical formulation of the adjoint sensitivity analysis, its results, and a comparison with RTM WFs. Section 3 also overviews the quality control methodology employed for this work. Section 4 follows with an overview of the mesoscale forecast verification procedure and results. Section 5 covers the conclusions and future work.

2. The AIRS data, RTM, test cases, and forecast models

a. The AIRS data

AIRS, one of the many instruments carried on board the National Aeronautics and Space Administration's (NASA) *Aqua* satellite, is a hyperspectral infrared sounder capable of collecting 2378 thermal infrared radiance observations across a spectrum from 3.7 to 15.4 μm . The cross-track swath dimension is 1650 km. The spatial resolution for AIRS is 13.5 km at nadir (Aumann et al. 2003).

AIRS level 1B radiance data are available in hierarchical data format (HDF) from the Goddard Earth Sciences Data and Information Services Center (GES DISC). AIRS data from each day are structured in 6-min swath packages known as granules. Since the *Aqua* satellite is sun-synchronous, the data are available globally, twice daily at the same local times each day. The level 1B radiance data consist of calibrated radiances assigned to each wavenumber in the spectrum. The radiances are converted into BTs here with the inverse of the Planck function. Noisy and/or popping channels (i.e., channels whose BT values "pop" to high values suddenly without any gradual transition) as specified by several onboard calibration tests (space view test, onboard calibration cool-down test, etc.) are removed using the quality control package available with the AIRS radiance packages. For further information regarding the AIRS instrument, see Pagano et al. (2002).

b. The radiative transfer model and its adjoint

The RTM selected for this work is the Stand-alone AIRS Radiative Transfer Algorithm (SARTA; Strow et al. 2003). SARTA calculates radiance and BT values for two pixels each second (on an SGI Origin machine), with errors near that of the AIRS instrument itself (about 0.2 K at 250 K) (Strow et al. 2003). SARTA is designed to calculate a simulated AIRS radiance spectrum as the convolution of the monochromatic radiance with the AIRS spectral response function (SRF) for any specified AIRS channel. The model does not have the capability to resolve scattering effects, and as such considers only four source terms: surface emission, atmospheric emission, downwelling atmospheric emission reflected by the surface, and reflected solar radiation. The SARTA package includes an additional program suite, known as kLAYERS, to interpolate input data from N model levels to the 100 layers needed by SARTA. Linear interpolation (on $\log P$ levels, where P is pressure) is used by kLAYERS to convert input profile data to 101 levels from the surface to 0.0050 hPa. Then, kLAYERS converts atmospheric profiles at discrete point levels onto 100 fixed integrated slab layers used in SARTA. For those layers that are above the top of the input data (in our case above 50 hPa), kLAYERS merges a reference profile (based on the latitude and time of year of the input profile) to fill in for missing data.

The surface emissivity and reflectivity values are fed into SARTA from a set of reference points (obtained from the AIRS observation file). These reference emissivity and reflectivity values are interpolated (or extrapolated) onto the AIRS channel wavelengths. Interpolations are linear in wavelength. Problems remain with the use of these values over land; this is addressed later in section 4a. Details on the model's radiative transfer algorithm and how to calculate each term can be found in Strow et al. (2003).

To formulate the adjoint of the forward RTM, the RTM must first be linearized around a basic state (e.g., the nonlinear state) to obtain the so-called tangent linear RTM. The nonlinear RTM can be expressed as

$$T_b^\alpha = H_\alpha(\mathbf{x}), \quad (1)$$

where H is the operator (RTM) with the input vector \mathbf{x} to produce T_b^α (the brightness temperature at channel α). The tangent linear model of (1) is simply

$$\delta T_b^\alpha = H_\alpha(\mathbf{x})\delta\mathbf{x}, \quad (2)$$

where $H_\alpha = \partial H_\alpha / \partial \mathbf{x}$ is the tangent linear operator of RTM producing the perturbed BT values (δT_b^α) for a given perturbation in input vector \mathbf{x} ($\delta\mathbf{x}$). The computer

program for the tangent linear RTM is obtained by linearizing every line of the computer code that composes the RTM by a sequence of differentiations with respect to the input variables \mathbf{x} and any variables that are functions of \mathbf{x} .

The adjoint RTM can be expressed as

$$\hat{\mathbf{x}} = H_\alpha^T(\mathbf{x})\hat{T}_b^\alpha, \quad (3)$$

where H_α^T is the transpose of H_α and is called the adjoint operator, \hat{T}_b^α is the adjoint variable of BT, and $\hat{\mathbf{x}}$ is the adjoint variables of \mathbf{x} . For different applications of the adjoint RTM, different values will be given to \hat{T}_b^α (see section 3a). The computer program for the adjoint RTM is based directly on the tangent linear RTM program, realizing the transpose of the tangent linear model. The sequence of operations and the input and output in the tangent linear RTM is reversed for the adjoint RTM. However, the basic state calculations needed in the adjoint operator keep the same sequence as in the tangent linear code.

The accuracy of the tangent linear RTM is verified against the nonlinear RTM, and subsequently the accuracy of the adjoint RTM is verified against the tangent linear RTM. Both the tangent linear and adjoint models have been deemed accurate within the precision of the computer, in this case 13 digits on an SGI Origin.

c. A quality control procedure

Cloud contamination is a major problem when dealing with infrared sounder data and when using an RTM that does not account for cloud effects, such as SARTA. Therefore, cloud-contaminated BTs must be removed from consideration. To ensure that only high quality data are being used for the verification of the fifth-generation Pennsylvania State University–National Center for Atmospheric Research Mesoscale Model (MM5) forecasts, a quality control procedure developed by Carrier et al. (2007) is applied. It implements a limited cloud-contaminated data removal (LCCDR) algorithm to remove cloud-contaminated BTs as well as those remaining observations that differ significantly from the simulated BT values.

The LCCDR algorithm examines the weighting function profile for each AIRS channel, at each AIRS footprint, to determine a channel-dependent cutoff pressure (COP) level, which is a level above which the emission is no less than $\frac{1}{3}$ of the total value. The COP level for each channel is then compared with the cloud-top pressure from the Moderate Resolution Imaging Spectroradiometer (MODIS). If a channel's COP level is below the MODIS cloud top, that channel is discarded. Finally, the biweight method (Lanzante 1996) is used to

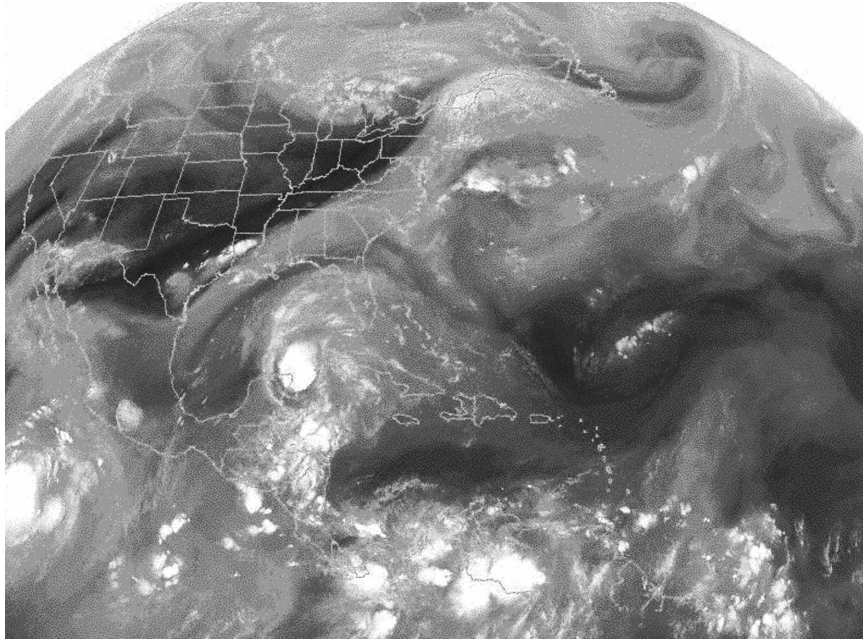


FIG. 1. *GOES-12* midlevel water vapor image from 1200 UTC 11 Jul 2003. Area of interest is the southeastern United States and the midlevel moisture gradient present at this time. Image courtesy of NCDC Satellite Browse Archive (information online at <http://www.ncdc.noaa.gov/oa/satellite/satellitedata.html>.)

remove those remaining data points that deviate significantly from simulated radiances in consideration of potential error in the MODIS cloud-top estimates and in the determination of the COP level. The biweight method first calculates the biweight mean and the standard deviation, which are more resistant to outliers than those calculated by the standard method. The biweight mean and standard deviation are then used for identification of outliers.

The results from this quality control procedure have shown that many channels from cloudy fields of view (FOVs) that would have otherwise been discarded are retained. The error analysis also suggests that the data retained from our algorithm possess the same (and at times, better) error characteristics as those channels from completely clear FOVs (Carrier et al. 2007).

d. Test case and forecast model

The test case involves a strong middle- and upper-level moisture gradient associated with a cold front over the southeastern United States on 11 July 2003. This case was selected because of its simplicity, as there is minimal cloudiness and no large-scale precipitation over the southeastern United States during this time. Figure 1 shows a *Geostationary Operational Environmental Satellite-12 (GOES-12)* midlevel water vapor image at 1200 UTC 11 July 2003. The midlevel moisture

gradient is visible within the region of interest (over the southeastern United States).

Version 3 of the MM5 is used here (Dudhia 1993). The 36-h forecast, initialized at 0000 UTC 11 July 2003, has a domain centered over St. Louis, Missouri, with a grid size of $150 \times 150 \times 35$, a horizontal resolution of 20 km, and a model top at 50 hPa (Fig. 2). The Grell cumulus convective scheme (Grell et al. 1995) and Blackadar planetary boundary layer (Blackadar 1979) are used in this forecast. The size of the forecast domain is large enough to cover the southeastern United States (the region of interest) while also overlapping a majority of the AIRS pixels from two different swath times: 0747 UTC 11 July (AIRS granule 078) and 1847 UTC 11 July (AIRS granule 188). Granule 078 is a local nighttime period, and the 8-h forecast is used for input to SARTA; granule 188 is a local daytime period, and the 19-h forecast is used as input to SARTA. AIRS data from granule 078 and MM5/SARTA data from the 8-h forecast will be referred to as T1; AIRS data from granule 188 and MM5/SARTA data from the 19-h forecast will be referred to as T2. The spatial coverage of both swaths is shown in Fig. 2.

3. Adjoint sensitivity study

When verifying model forecasts against AIRS radiance observations, it is important to know which me-

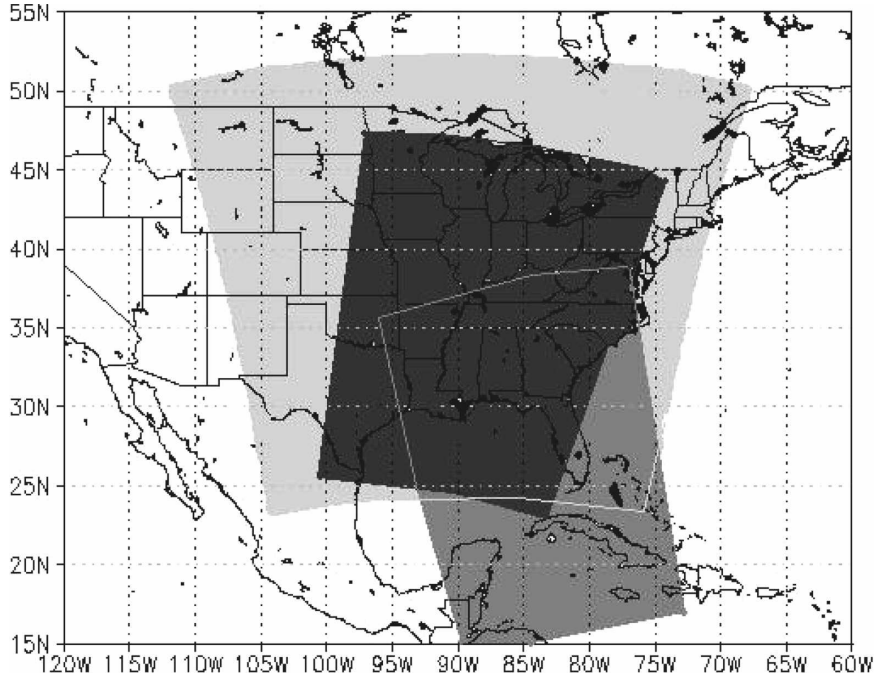


FIG. 2. MM5 forecast domain, for the MM5 forecast initialized at 0000 UTC 11 Jul 2003, with a grid size of $150 \times 150 \times 35$ with 20-km resolution (light gray region). AIRS scan swath at 0747 UTC 11 Jul 2003 (granule 078) is in dark gray shading. AIRS scan swath at 1847 UTC 11 Jul 2003 (granule 188) is in medium gray shading.

teological variable, at what level, has the greatest influence on the simulation of specific RTM spectral channels. An adjoint sensitivity study of AIRS radiances will provide such information based on the relative sensitivities of each RTM channel BT to each MM5 forecast variable (input to the RTM).

a. Formulation and results of the adjoint sensitivity study

For a sensitivity study of BT, the response function is simply defined as

$$R_\alpha(\mathbf{x}) = T_b^\alpha. \tag{4}$$

The adjoint RTM is used to first obtain the gradient of R_α with respect to the atmospheric variable \mathbf{x} , $\nabla_{\mathbf{x}}R_\alpha$, by setting

$$\hat{T}_b^\alpha = \frac{\partial R_\alpha}{\partial T_b^\alpha} \equiv 1 \tag{5}$$

in (3). The resulting value after applying the adjoint RTM (3) is the gradient $\hat{\mathbf{x}}$:

$$\hat{\mathbf{x}} = \nabla_{\mathbf{x}}R_\alpha. \tag{6}$$

The sensitivity of the BT with respect to the input vector \mathbf{x} can then be calculated according to the following formula:

$$R_\alpha^{\text{sens}} = (\nabla_{\mathbf{x}}R_\alpha)^T \delta \mathbf{x} \equiv (\hat{\mathbf{x}})^T \delta \mathbf{x}. \tag{7}$$

If there is a variation only in the l th component of \mathbf{x} , that is,

$$\delta \mathbf{x} \equiv \delta \mathbf{x}^l = \begin{pmatrix} 0 \\ \vdots \\ \delta x^l \\ \vdots \\ 0 \end{pmatrix}, \tag{8}$$

the corresponding sensitivity can be written as $R_\alpha^{\text{sens}-l} = (\hat{\mathbf{x}})^T \delta \mathbf{x}^l$.

To compare the sensitivity of BT with both temperature and specific humidity at different vertical levels, the following nondimensional relative sensitivity must be used (Zou et al. 1993):

$$s_\alpha^l = \frac{R_\alpha^{\text{sens}-l}}{R_\alpha} \left(\frac{\delta x^l}{x^l} \right)^{-1} \equiv \frac{\hat{x}^l x^l}{R_\alpha}, \tag{9}$$

where $\delta \mathbf{x}^l = (0, \dots, \delta x^l, \dots, 0)^T$ is a perturbation vector where only the l th component of \mathbf{x} is perturbed,

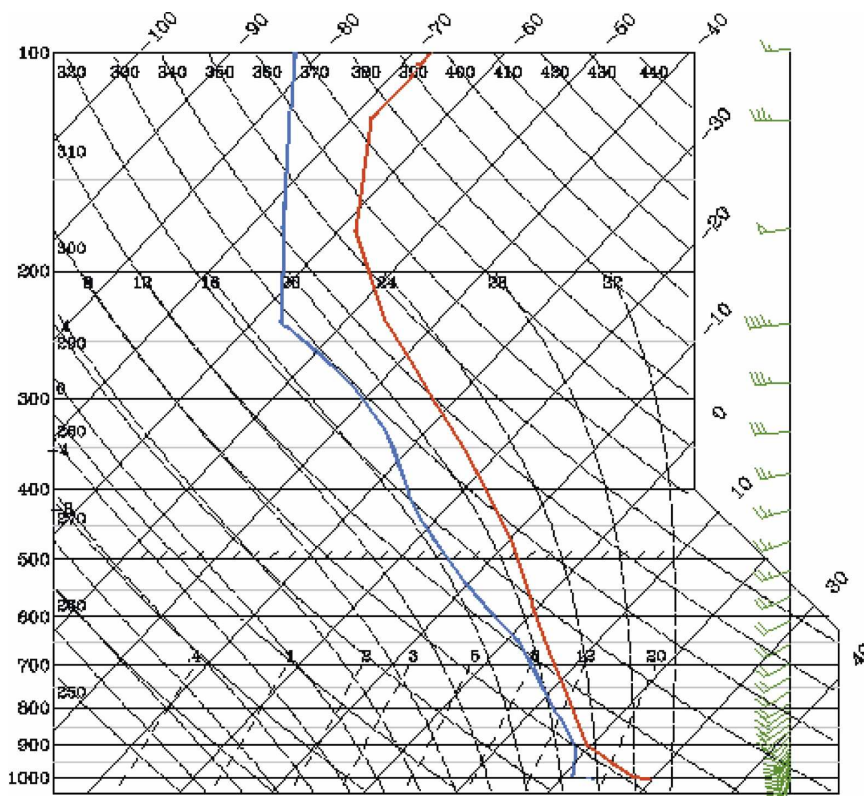


FIG. 3. MM5 temperature (red) and mixing ratio (blue) vertical profiles from the clear-sky domain point (33.2°N, 86.8°W) used for example adjoint sensitivity study. Green wind barbs show wind speed and direction at each pressure level. Data are from T1 (8-h MM5 forecast initialized at 0000 UTC 11 Jul 2003).

$R_{\alpha}^{\text{sens-}l} = (\hat{\mathbf{x}})^T \delta \mathbf{x}^l$ is the sensitivity resulting from perturbation $\delta \mathbf{x}^l$, and $\hat{\mathbf{x}}^l$ is the gradient of the response function R_{α} with respect to the l th input variable of \mathbf{x} . The relative sensitivity

$$\mathbf{s}_{\alpha} = \begin{pmatrix} s_{\alpha}^1 \\ s_{\alpha}^2 \\ \vdots \\ s_{\alpha}^N \end{pmatrix} \quad (10)$$

is nondimensional and is found by a vector multiplication of the adjoint variable $\hat{\mathbf{x}}$ and input variable \mathbf{x} of R_{α} , divided by the response function [see (9)].

The magnitude of the relative sensitivity signifies the importance of each input variable for each spectral channel. To judge whether the radiance is more sensitive to temperature or specific humidity, one can simply plot the relative sensitivity \mathbf{s}_{α} . The relative sensitivity of the BT to atmospheric temperature (RS- T) and specific humidity (RS- Q) at specific vertical levels can also be investigated. This is particularly useful when trying to

quantify which channels to use for data assimilation or when trying to investigate error in the model response and/or input variables using AIRS radiance observations.

The sign of the relative sensitivity is also important. It signifies how the input parameter can affect the RTM response. For instance, positive (negative) sensitivity of BT suggests that increasing (decreasing) the value of the input variable will lead to an increase (decrease) in the BT value.

Figure 3 shows the vertical profile of the temperature and mixing ratio used as the input field (\mathbf{x}) for the WF and adjoint sensitivity calculations. This profile is at an MM5 grid point (33.2°N, 86.8°W) located in southern Alabama. This profile indicates somewhat dry conditions near the surface until about 900 hPa when the sounding becomes wetter.

Figure 4 shows the maximum values of RS- T (brown, values on left y axis) and RS- Q (black, values on right y axis) for the first 1864 AIRS channels. The maximum value of the RS- T at each channel is positive, whereas the maximum RS- Q values are all negative, as would be

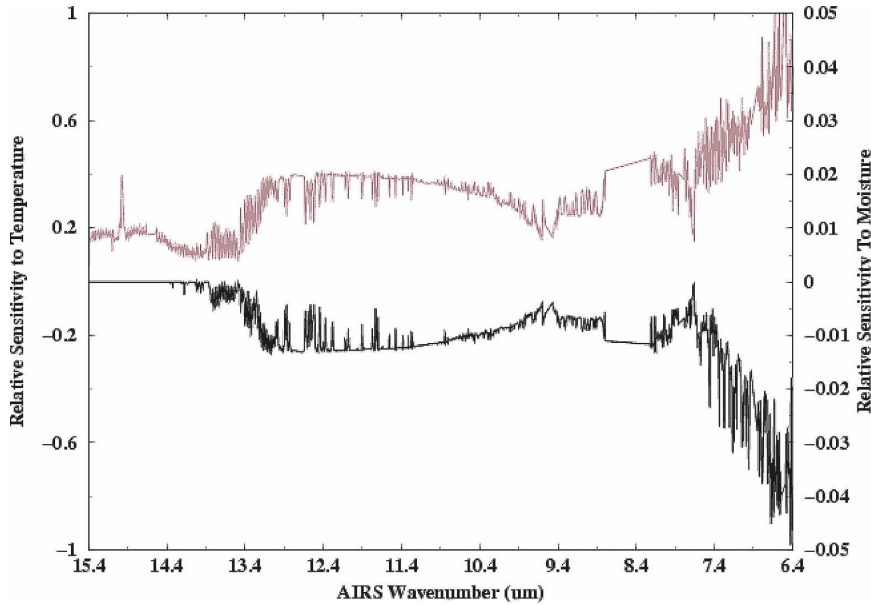


FIG. 4. Maximum sensitivity values at each AIRS wavelength for T1 sensitivity analysis (using 8-h MM5 forecast initialized at 0000 UTC 11 Jul 2003). The maximum RTM relative sensitivity to atmospheric temperature ($RS-T$) is in brown (values on left y axis), and maximum RTM sensitivity to specific humidity ($RS-Q$) is in black (values on right y axis). Values are dimensionless.

expected. The magnitude of the $RS-T$ is higher than that for $RS-Q$, indicating that the BT calculation is most sensitive to changes in the temperature variable than in the moisture variable, not only for the so-called carbon dioxide channels ($\lambda > 13.0 \mu\text{m}$), but also for the water vapor channels as well ($\lambda < 9.2 \mu\text{m}$). It is also apparent that the $RS-Q$ values in the water vapor channels are larger than those in other channels, indicating the increased importance of water vapor to the BTs in this spectral range. Overall, this result indicates that the simulated BT values would be impacted more by a change in the temperature than they would by a change in the moisture for the entire spectrum, and more by a change in the water vapor channels than in other channels.

To illustrate the vertical levels at which the relative sensitivity is highest, we show in Figs. 5–7 the $RS-T$ [(b) panels] and $RS-Q$ profiles [(c) panels] for three AIRS spectral ranges: 15.39–13.22 μm , a carbon dioxide band (Fig. 5); 12.34–8.79 μm , a window channel band (Fig. 6); and 8.22–6.20 μm , a water vapor band (Fig. 7). $RS-T$ values have been normalized and the $RS-Q$ values have been scaled up by 33%. The vertical levels are shown in log- P form on the vertical axis and the AIRS channel (in μm) on the horizontal axis. The $RS-Q$ values for the channels in this range are very low, indicating their relatively weak contribution to the radiance calculations for the carbon dioxide channels.

Figure 6 shows the comparison for the window channel band. Here, the peak $RS-T$ values lie near the surface (1042 hPa), but for each channel the sensitivity remains high, even slightly above the surface layer. This range of channels also exhibits high sensitivity to the surface skin temperature variable ($RS-TG$; Fig. 6, bottom panel). The $RS-Q$ values for this range are still rather low, as expected for window channels. Also, there is a slight increase in $RS-T$ values for atmospheric levels above 500 hPa between 9.78–9.27 μm in response to the ozone band. The $RS-TG$ value is higher for each window channel than the $RS-T$ value is by at least an order of magnitude (not shown). For example, the peak $RS-T$ value for channel 800 (10.85 μm) is 0.262155, whereas the $RS-TG$ value is 2.83521.

Figure 7 shows the comparison for the water vapor band. Here, the structure of the $RS-T$ and $RS-Q$ values match quite closely at each channel. Relatively high $RS-Q$ values exist in this band, suggesting that the specific humidity values are relatively important for these channels, as would be expected. However, the sensitivity analysis suggests that the temperature parameter is also relatively important to the radiance calculation for the water vapor band. It is therefore important to consider both the temperature channels and water vapor channels when attempting to obtain both profiles of temperature and moisture from AIRS BT data.

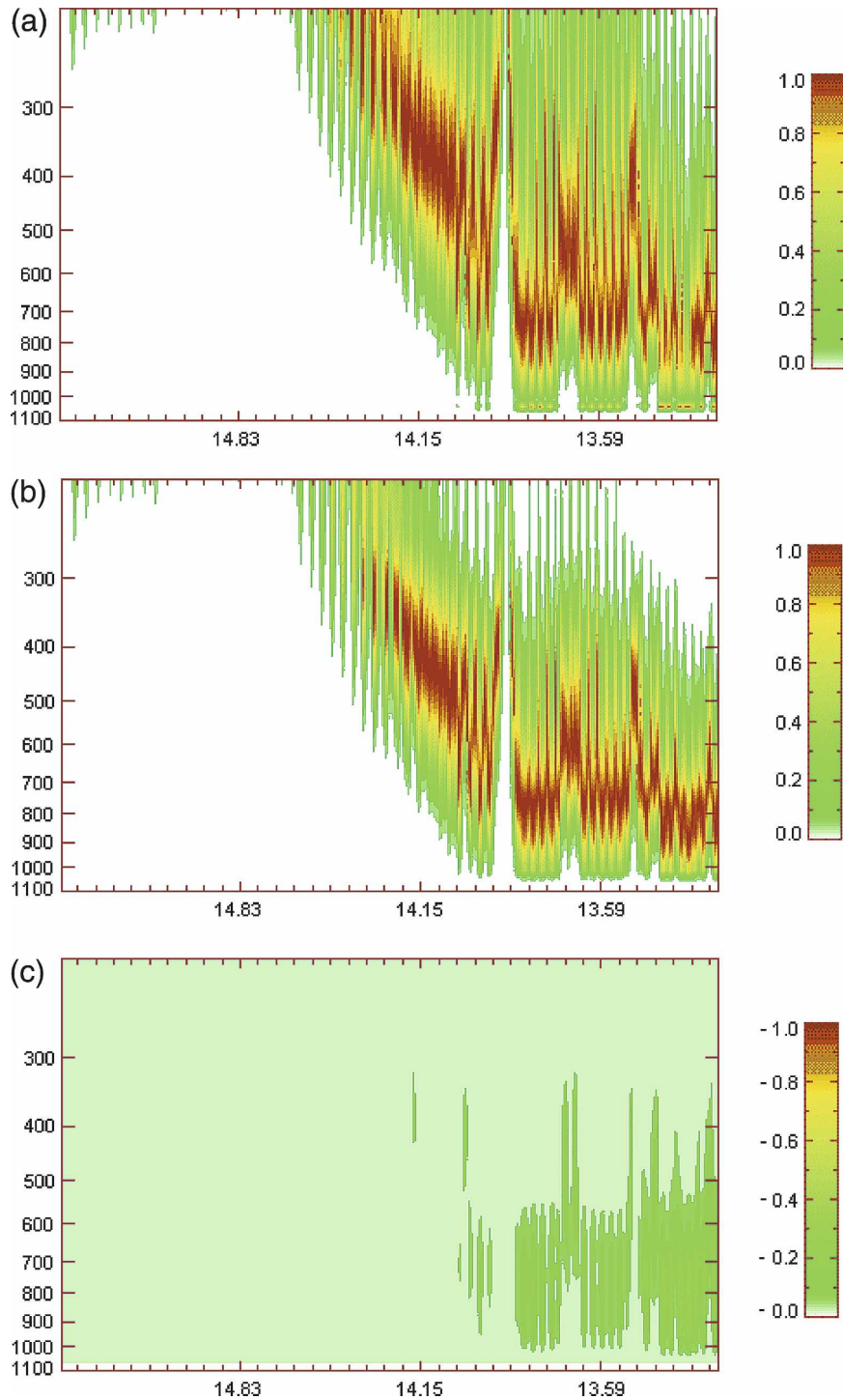


FIG. 5. RTM-normalized (a) WFs and (b) BT sensitivities to atmospheric temperature, and (c) specific humidity for the AIRS spectral range between 15.39 and 13.22 μm for T1 sensitivity analysis (using MM5 8-h forecast initialized at 0000 UTC 11 Jul 2003). Pressure levels are shown along the vertical axis, and AIRS wavelengths are shown along the horizontal axis; WFs and sensitivities are normalized.

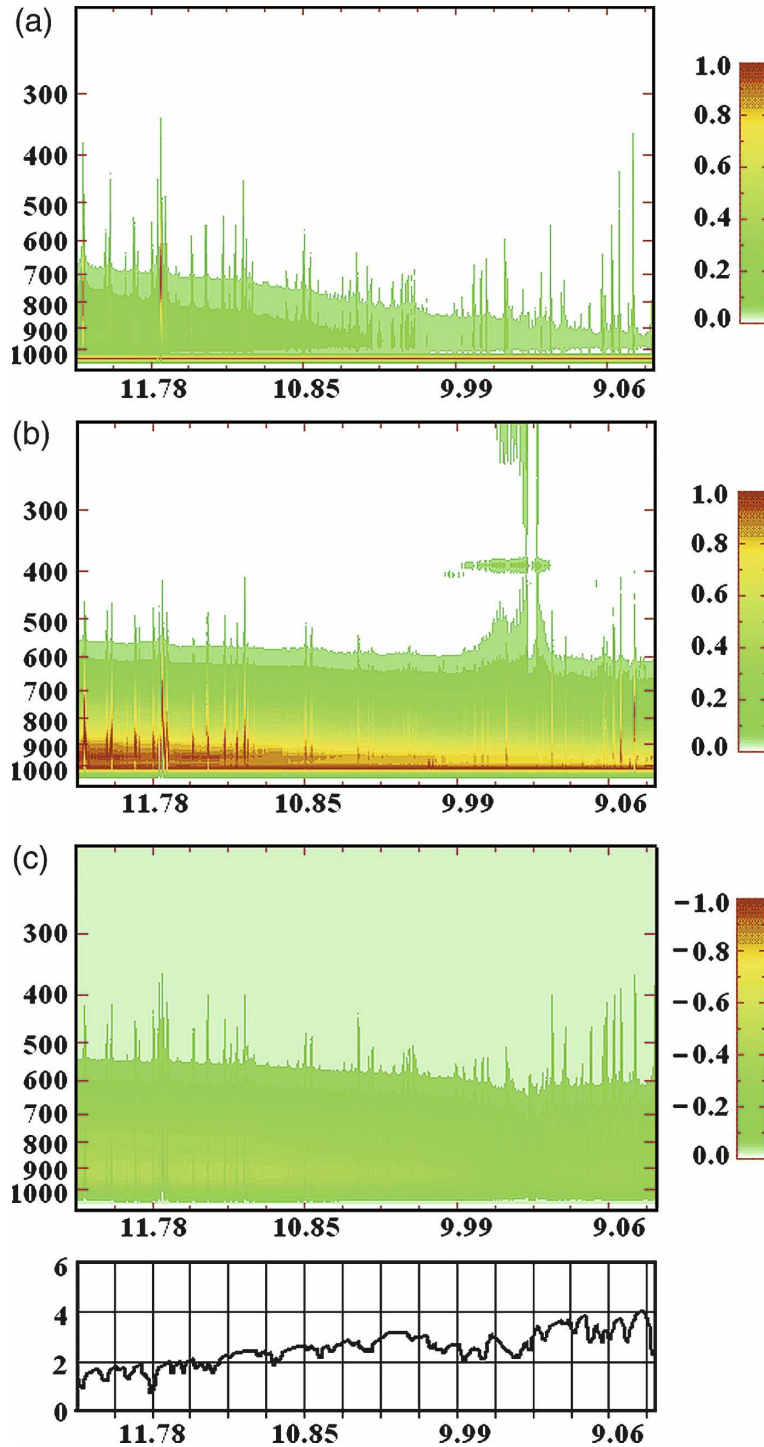


FIG. 6. (a)–(c) As in Fig. 5, but for spectral range 12.34–8.79 μm . (d) The sensitivity of BT to MM5 surface skin temperature variable (nondimensional relative sensitivity is shown along the y axis; AIRS channel is shown along the x axis).

b. RTM weighting functions

The WF quantifies the contribution of emissions from each atmospheric level and the total emission at

the top of the atmosphere for each channel. Therefore, the height of the maximum WF of radiance in a particular channel provides information on which atmospheric layer contributes the most to the measured ra-

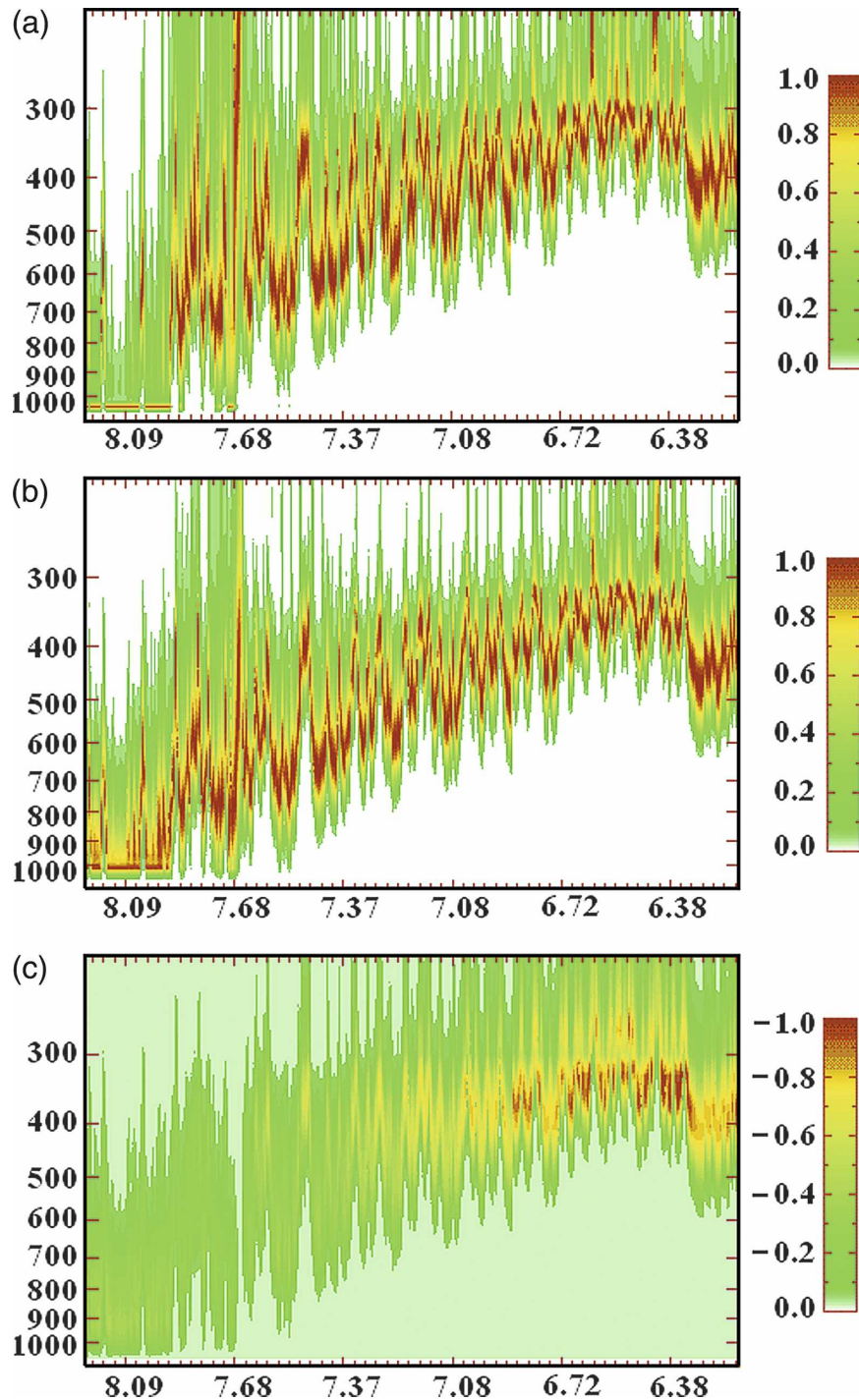


FIG. 7. As in Fig. 5, but for spectral range 8.22–6.20 μm .

diance. The broadness of the WF reflects the thickness of the atmospheric layer contributing most significantly to the measured radiance. On the other hand, as discussed above, the relative sensitivity provides information about which variable and at what height the radiance is most sensitive. Is the height at which BT is most

sensitive to temperature the same as that for specific humidity? Is the maximum WF height the same as the height where the relative sensitivity is highest? These are important questions relevant to many applications of AIRS radiance, such as targeted observations, data assimilation, and forecast verification.

Since the WF at a specific vertical level is representative of the amount of radiation emission at that level, which itself is a function of atmospheric temperature and moisture at, and above, that level, the BT can be approximately expressed as a weighted mean of the Planck function $[B(T)]$:

$$R_\alpha \equiv T_b^\alpha = \sum_l w_l^\alpha(T_1, T_2, \dots, T_l, q_1, q_2, \dots, q_l)B(T_l). \quad (11)$$

Variations in WF values from one level to another are much larger than the variations in the values of $B(T)$ are from one level to another. Therefore, the level where the WF value is the largest is the level at which the atmosphere contributes the most to the total radiation of that channel. However, the relative sensitivity finds the height where perturbations made to the most sensitive variable contribute the most to the first-order variation of BT:

$$R_\alpha^{\text{sens}} = \sum_k [\delta w_k^\alpha B(T_k) + w_k^\alpha \delta B(T_k)]. \quad (12)$$

In the second term in (12) the role of WF in the first-order variation of BT with respect to temperature perturbation, δT_l ($l = 1, 2, \dots, L$ vertical levels), is similar to its role in BT with respect to background temperature, T_l ($l = 1, 2, \dots, L$) [see (8)]. It is the first term in (12) that might contribute to a discrepancy between the maximum WF height and the height where the relative sensitivity is highest. For example, the sensitivity due to temperature perturbation at the k th level will be

$$R_\alpha^{\text{sens},l} = \left[w_l^\alpha \frac{dB}{dT} + \frac{\partial w_l^\alpha}{\partial T} B(T_l) \right] \delta T_l. \quad (13)$$

The relative sensitivity will be

$$s_\alpha^{\text{sens},l} = \frac{\left[w_l^\alpha \frac{dB}{dT} + \frac{\partial w_l^\alpha}{\partial T} B(T_l) \right] T_l}{T_b^\alpha} = \frac{w_l^\alpha \frac{dB}{dT} T_l + \frac{\partial w_l^\alpha}{\partial T} B(T_l) T_l}{T_b^\alpha}. \quad (14)$$

Based on the first term in (14), the height of the maximum sensitivity could be rendered lower (higher) than the height of the maximum WF if the temperature decreases (increases) with height near the maximum WF height. Also, since

$$\frac{\partial w_l^\alpha}{\partial T} \begin{cases} \geq 0 & \text{above the WF maximum height} \\ = 0 & \text{at the WF maximum height,} \\ \leq 0 & \text{below the WF maximum height} \end{cases} \quad (15)$$

the height of the maximum sensitivity could be rendered higher than the maximum WF height because of the contribution from the second term in (14). In the following, it is shown that the height at which BT is most sensitive to temperature could be different from that for specific humidity, and the maximum WF height could be different from the height where the relative sensitivity is highest.

Figure 8 shows the vertical heights of the maximum WF, RS- T , and RS- Q peaks for three AIRS spectral ranges: 14.83–14.15 μm , an upper-level carbon dioxide band (Fig. 8a); 14.14–13.59 μm , a midlevel carbon dioxide band (Fig. 8b); and 7.37–7.08 μm , a water vapor band (Fig. 8c). Clearly, the peak WF, RS- T , and RS- Q values do not always lie at the same atmospheric level. In fact, it appears that the peak RS- T value is vertically higher in the atmosphere than the WF peak for those channels whose maximum emission is above the tropopause (~ 200 hPa). Conversely, the peak RS- T value falls vertically below that for the WF at channels with peak emissions below 200 hPa. It is clear that those channels whose peak RS- T values lie vertically above the peak WF values have the maximum emission from above the tropopause within a region where the temperature increases with height. This is consistent with the theoretical prediction from (14).

The relationship between the vertical shift of RS- T levels from the peak WF and the sign of the vertical temperature gradient is further confirmed in Fig. 9 for all AIRS channels that exhibit a shift between the peak WF and RS- T levels. Figure 9 shows the relationship between the vertical shift between the peak WF and RS- T levels and the sign of the vertical temperature gradient at the level of the peak WF (the zero-value lines are shown in gray; negative vertical shift value represents an *upward* sensitivity shift relative to the WF profile). If the vertical temperature gradient is negative at the peak WF height, then the RS- T shift is downward (since the $\partial W_l^\alpha / \partial T$ term is negative in that direction); on the other hand, if the vertical temperature gradient is positive at the peak WF height, then the RS- T shift is upward (since the $\partial W_l^\alpha / \partial T$ term is positive in that direction). Figure 10 shows the relationship between the magnitude of the vertical shift in RS- T and the “broadness” of the WF profile (which is found to control the magnitude of the vertical shift). Open circles indicate those channels that exhibit an upward shift in the RS- T profile; closed circles indicate those channels that exhibit a downward shift in the RS- T profile. The broadness of the WF profile is defined by the thickness (in hPa) between the peak WF pressure level and the last pressure level with a WF value at or above 0.9, in the

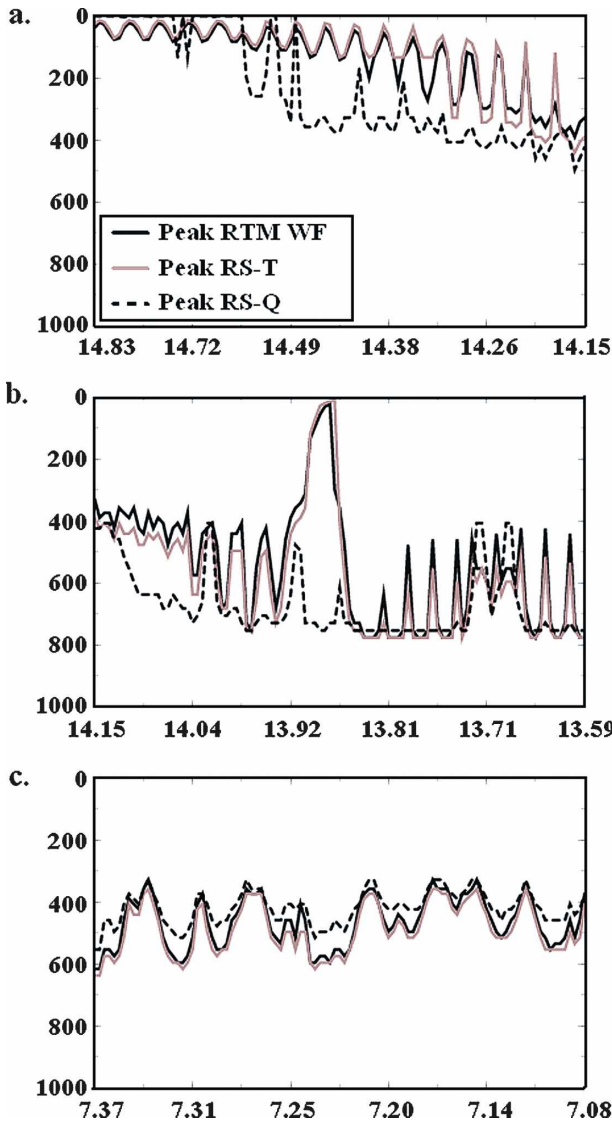


FIG. 8. Vertical levels of maximum BT sensitivity to atmospheric temperature (brown) and moisture (dashed) as well as the maximum WF height (black) for T1 (using 8-h MM5 forecast initialized at 0000 UTC 11 Jul 2003). Pressure level (hPa) is shown along the vertical axis; spectral channel (μm) is shown along the horizontal axis. Shown are spectral ranges between (a) 14.83 and 14.15 μm (carbon dioxide temperature channels), (b) 14.15 and 13.59 μm (window channels), and (c) 7.37 and 7.08 μm (water vapor channels).

direction of the RS-*T* shift. The channels that have the large shifts (>100 hPa) of the peak RS-*T* height from the maximum WF height are the midlevel carbon dioxide channels due to the broadness of these channels (not shown). “Upward-shifting” channels exhibit small shifts (open circles), since these channels, being in the stratosphere, are not very broad.

It has been shown that the vertical level where

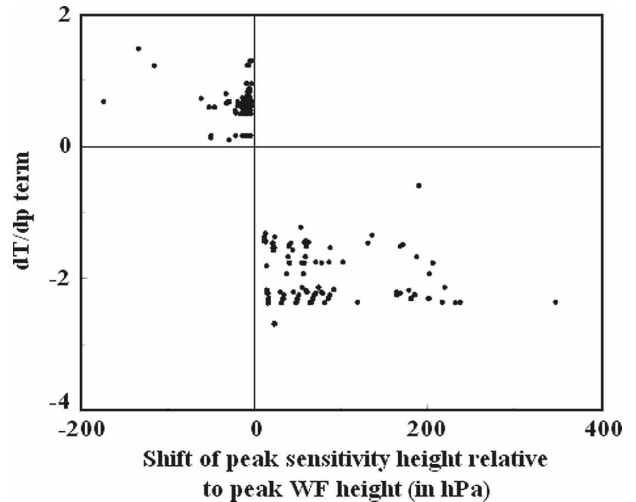


FIG. 9. Difference in pressure levels of the peak RTM WF and peak RTM RS-*T* (vertical shift) and the corresponding $d(T)/dp$ term at the level of peak RTM WF for G078-T2. Data shown here are from the same BT data used in the T1 sensitivity analysis (using 8-h MM5 forecast initialized at 0000 UTC 11 Jul 2003). Channels shown here are for all of those with peak WFs above 800 hPa (some data points overlap).

changes in the model state contribute mostly to the changes in the calculated radiance can be different from that suggested by the WF profile. This has direct applications for inferring which variable, at what level, might result in a model forecast error when radiance data is used for forecast verification.

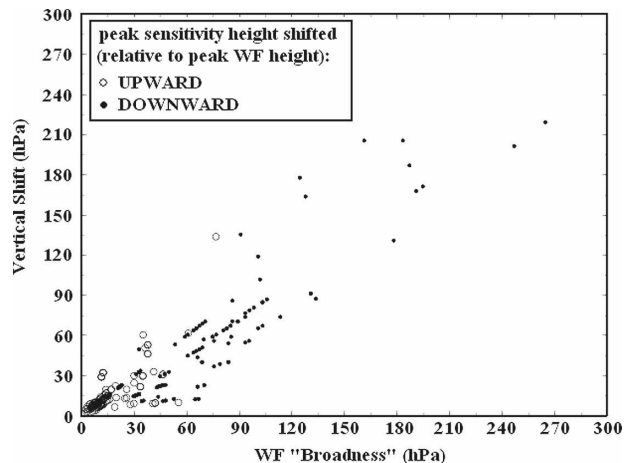


FIG. 10. Difference in pressure levels of the peak RTM WF and peak RTM RS-*T* (vertical shift, y axis) and the “broadness” of the RTM WF in the direction of the shift. Open circles indicate those channels that exhibit an upward RS-*T* peak shift (relative to the RTM WF peak). Closed circles indicate those channels that exhibit a downward RS-*T* peak shift (relative to the RTM WF peak). Data are from the T1 sensitivity analysis (using 8-h MM5 forecast initialized at 0000 UTC 11 Jul 2003).

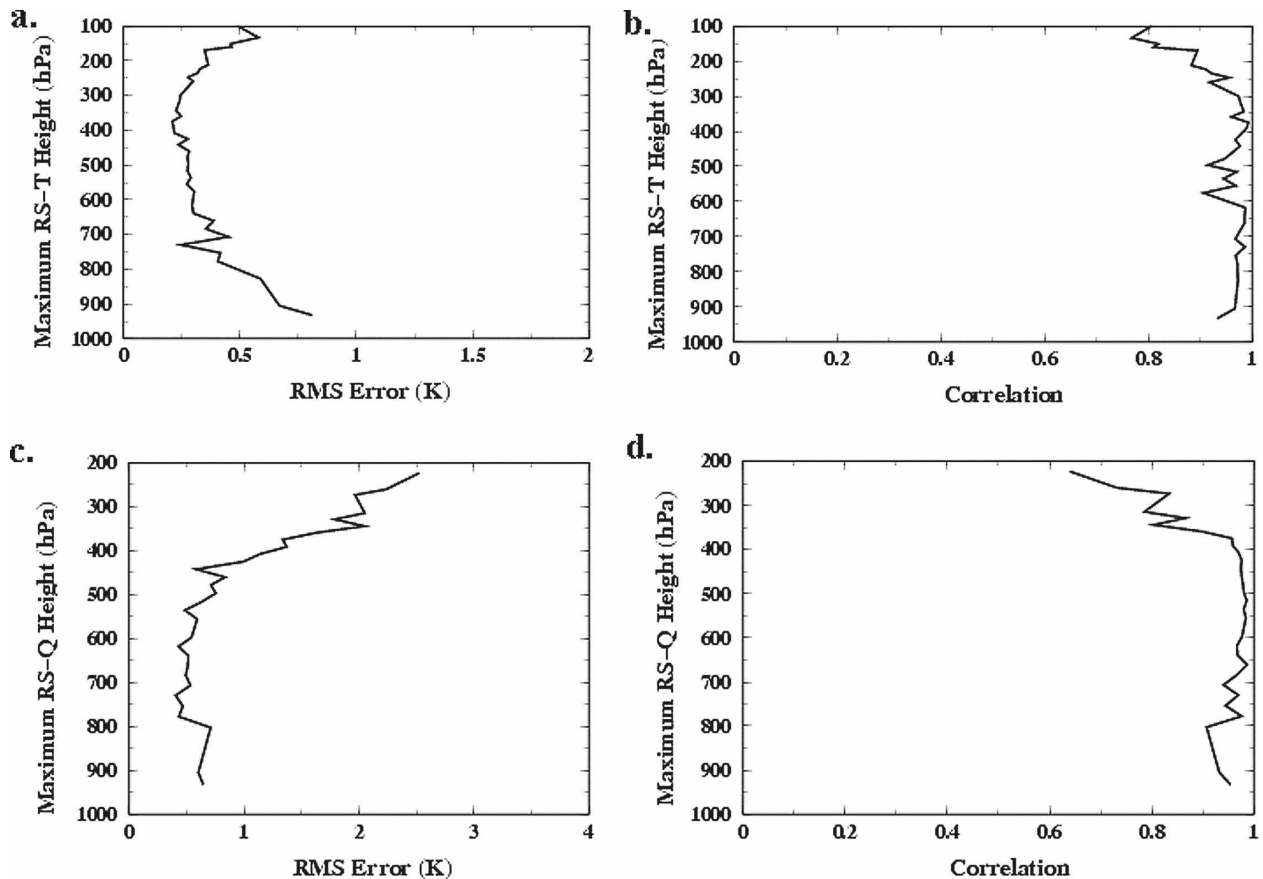


FIG. 11. (a), (c) RMS error and (b), (d) correlation coefficient of the simulated BTs using the MM5 forecast and AIRS data from T1 (8-h forecast). Here, (a), (b) show all the carbon dioxide and surface channels, and (c), (d) show water vapor channels. Channels are organized by (top) the maximum BT sensitivity to atmospheric temperature and (bottom) the maximum BT sensitivity to specific humidity.

4. Evaluation of a mesoscale forecast in light of the adjoint sensitivity results

Forecast verification using AIRS radiance data

Model-simulated and AIRS-observed BTs are compared to isolate and identify probable errors in the forecast model. The simulated BT values are calculated from the temperature and specific humidity forecasted by the model. The question is, how do we link differences found in radiance space to model variable space? In the following, we will show that the maximum relative sensitivity of radiance provides a way to do this.

To evaluate the MM5 forecast of temperature and specific humidity using AIRS BT data, the data are divided into two groups: (i) the carbon dioxide and surface channels and (ii) the water vapor channels. The root-mean-square (RMS) error and correlation calculated in BT space over the entire overlapping domain of AIRS data and the forecast model are calculated and presented as a vertical profile corresponding to the heights (in hPa) of the maximum relative sensitivity of

BTs to temperature and specific humidity for the two groups of BT data, respectively (Figs. 11 and 12). Cloud-contaminated data and outliers are removed a priori. A low-pass (boxcar) filter, applied in frequency space, is applied to the AIRS observations in order to reduce the observational noise. Since the AIRS observational and RTM errors (≈ 0.5 K for a 250-K scene) are known (Pagano et al. 2002; Strow et al. 2003), the error signal due to the MM5 forecast is conservatively set for RMS errors above 2.0 K.

Figures 11 and 12 show the RMS errors (left panels) and correlation coefficients (right panels) of BTs at different AIRS channels for T1 valid at 0800 UTC 11 July 2003 and for T2 valid at 1900 UTC 11 July 2003, respectively. Figures 11a,b and 12a,b include all of the carbon dioxide and surface channels and Figs. 11c,d and 12c,d include the water vapor channels. The BT data in the carbon dioxide and surface channels have been sorted by their corresponding heights (hPa) of the maximum relative sensitivity of BTs to temperature (Figs. 11a,c and 12a,c), and the BT data in the water

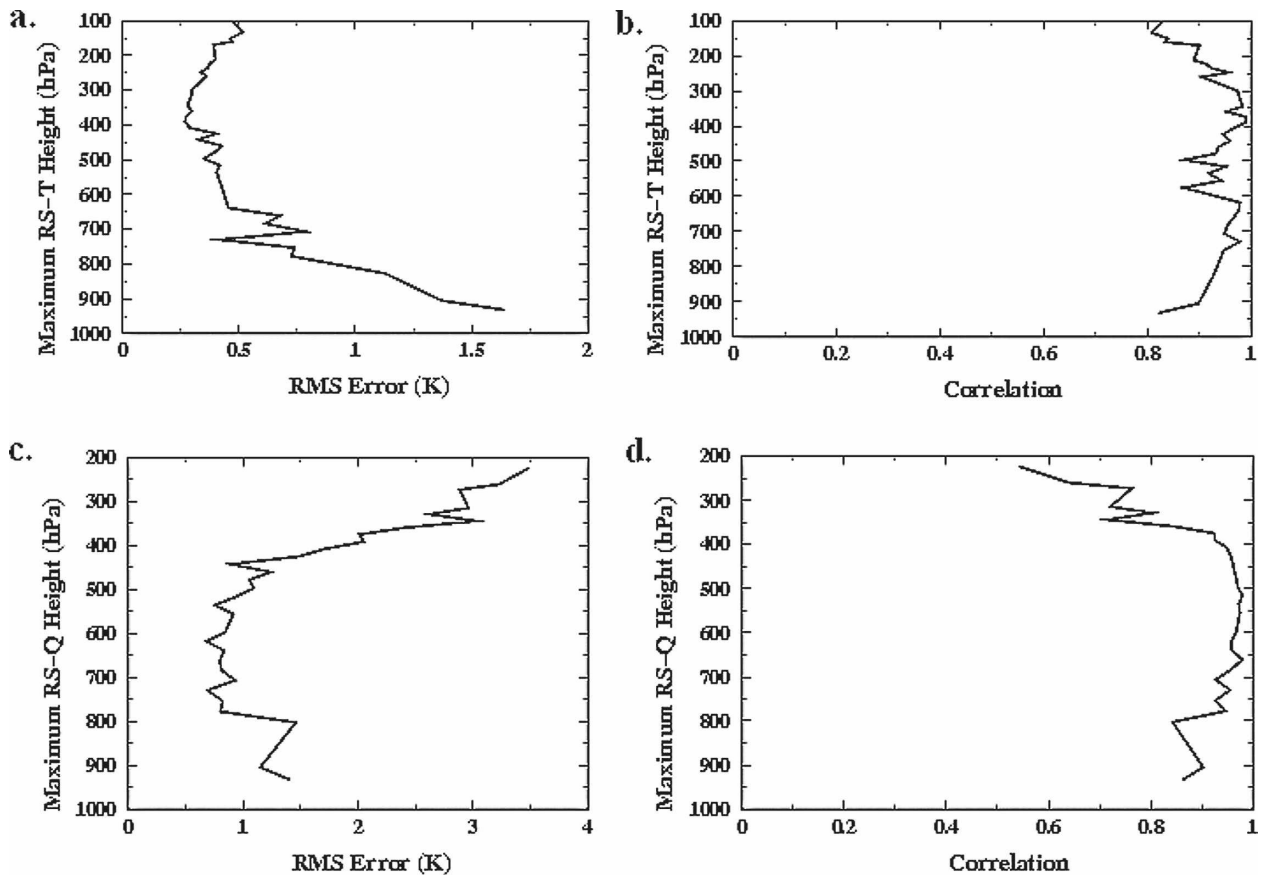


FIG. 12. As in Fig. 11, but for the MM5 forecast and AIRS data from T2 (18-h forecast).

vapor channels are sorted by the vertical heights of the maximum relative sensitivity of BTs to specific humidity (Figs. 11b,d and 12b,d). Since these channels have not been arranged by wavelength, Figs. 13 and 14 show the corresponding wavelengths (Fig. 13) and observed mean brightness temperatures (Fig. 14) of all data used in Figs. 11 and 12. Figure 13 indicates which set of channels is used in the error plots in Figs. 11 and 12. Channels whose peak sensitivity (RS- T and RS- Q) values are located in the higher atmosphere have, in general, lower BTs (Fig. 14).

Examining the carbon dioxide channels for RMS error (Figs. 11a and 12a), one can see that the RMS error is below 1 K. Figure 12a shows a slightly elevated near-surface channel error, which is most likely due to errors in surface emissivity or other surface effects (i.e., error in MM5 model surface skin temperature), or a combination of both. For those near-surface channels, or for channels with a significant surface contribution, it is rather difficult to separate the forecast model error from total error, since errors in the RTM could be significant because of errors in the specification of the surface state (e.g., surface emissivity and reflectivity)

during overland scenarios (McNally et al. 2006). For this reason it is best to include only those channels that have little or no surface contribution to overland FOVs for forecast verification purposes. In any case, the error associated with carbon dioxide channels above the surface for both cases is relatively low (Figs. 11a and 12a), indicating that the MM5 temperature forecast is closely approximating the atmospheric state depicted by the AIRS observations. The error associated with water vapor channels is relatively low (below 1 K) below 500 hPa (Figs. 11c and 12c). Between 200 and 400 hPa, however, an increase in RMS error with height is observed, with values approaching 2.5 K at 200 hPa for T1 (nighttime, an 8-h forecast) and 3.5 K for T2 (daytime, an 18-h forecast). This indicates a problem with the MM5 forecasts in the upper-tropospheric moisture fields associated with this middle- and upper-level moisture gradient case, which is discussed in more detail later (Figs. 16–18).

The correlation coefficients for the carbon dioxide and window channels for the two cases (Figs. 11b and 12b) show a similar pattern where the correlation in the upper levels (<200 hPa) is relatively low (<0.9), fol-

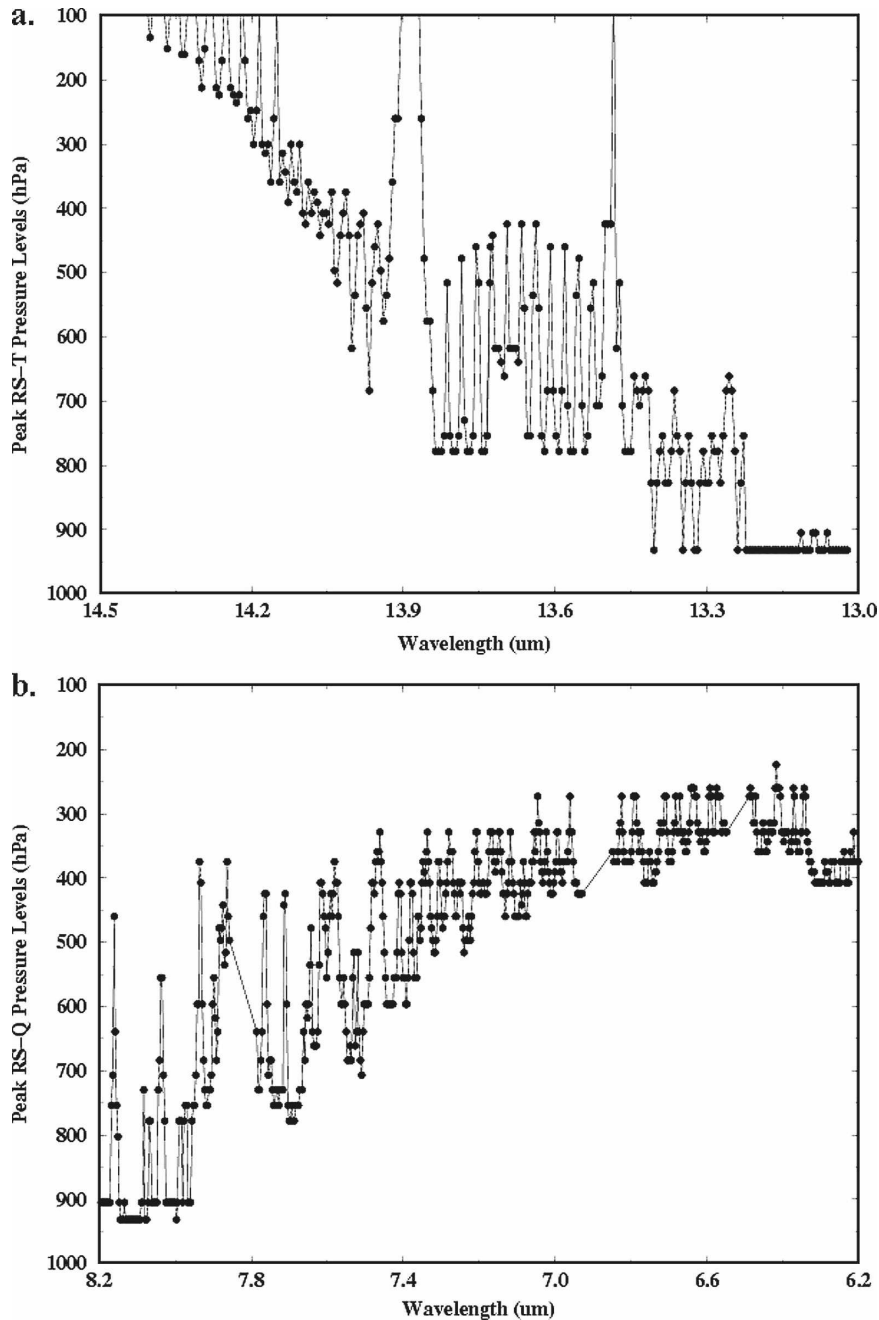


FIG. 13. (a) Peak RS- T pressure levels for the carbon dioxide channels and (b) peak RS- Q pressure levels for the water vapor channels. Channels in (a) are used for the statistical analysis shown in Figs. 11a,b and 12a,b. Channels in (b) are used for the statistical analysis shown in Figs. 11c,d and 12c,d. Data are from the T1 MM5/SARTA simulation (using an 8-h MM5 forecast initialized at 0000 UTC 11 Jul 2003).

lowed by a stretch of channels (with peak RS- T between 200 and 800 hPa) whose correlations are near or above 0.9. For those channels with a peak RS- T near the surface in T2, the correlation drops off slightly, likely due to the influence of surface skin temperature

error in MM5 and/or RTM emissivity error. The plotted correlations for the water vapor channels are relatively low for those channels whose peak RS- Q values are between 200 and 400 hPa (Figs. 11d and 12d). These results suggest that the MM5 is not simulating the layer

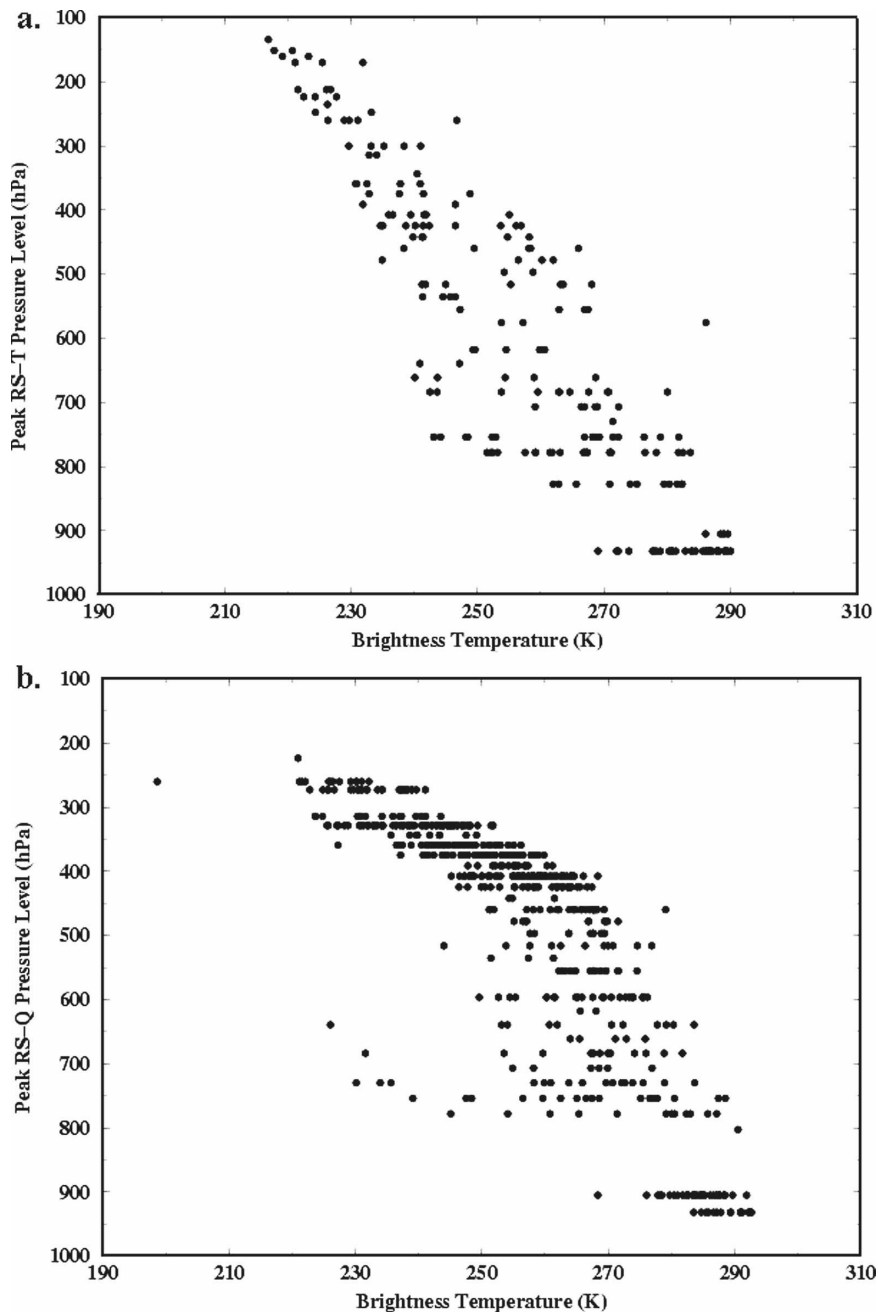


FIG. 14. BTs for (a) carbon dioxide channels (arranged by peak RS- T pressure level) and (b) water vapor channels (arranged by peak RS- Q pressure level). Channels in (a) are used for the statistical analysis shown in Figs. 11a,b and 12a,b. Channels in (b) are used for the statistical analysis shown in Figs. 11c,d and 12c,d. Data are from the T1 MM5/SARTA simulation (using an 8-h MM5 forecast initialized at 0000 UTC 11 Jul 2003).

above 400 hPa as well as the layer between 400 and 900 hPa.

In the following, three channels have been selected to examine model performances in capturing the spatial distributions of BTs observed by AIRS observations: an upper-level CO₂ channel (channel 209, 14.09 μm)

with the maximum sensitivity located at 330 hPa, a middle-level water vapor channel (channel 1583, 7.13 μm) with the maximum sensitivity located at 600 hPa, and an upper-level water vapor channel (channel 1752, 6.57 μm) with the maximum sensitivity located at 310 hPa (note: the qualitative description of “upper” or

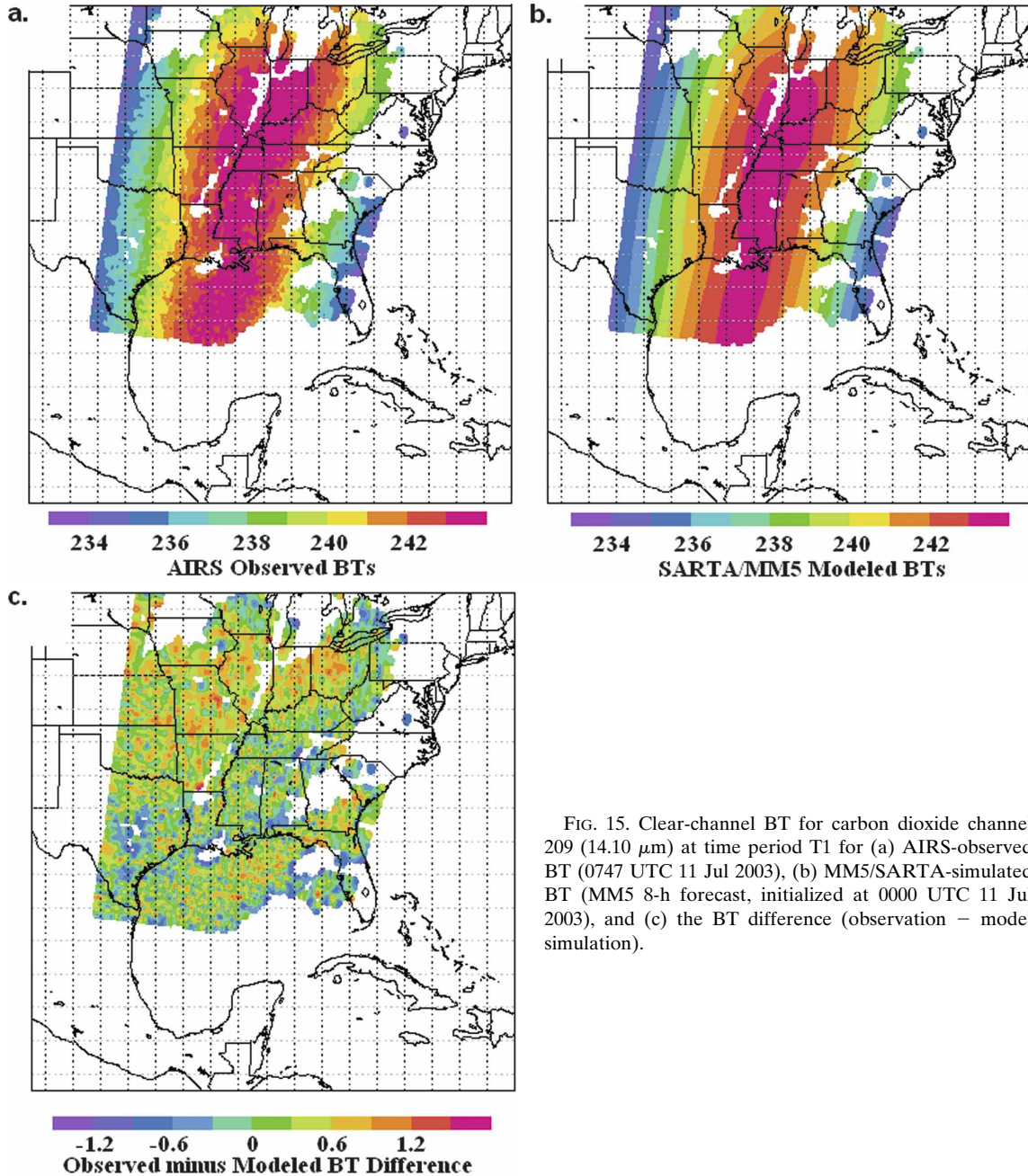


FIG. 15. Clear-channel BT for carbon dioxide channel 209 ($14.10 \mu\text{m}$) at time period T1 for (a) AIRS-observed BT (0747 UTC 11 Jul 2003), (b) MM5/SARTA-simulated BT (MM5 8-h forecast, initialized at 0000 UTC 11 Jul 2003), and (c) the BT difference (observation – model simulation).

“lower” channels is relative to the MM5’s model domain, not the AIRS instrument). Figure 15a displays the AIRS BTs and Figure 15b shows the MM5/SARTA BTs for channel 209 in the T1 case. Channel 209 is shown here as an example of a carbon dioxide channel, with peak emission within the 300–500-hPa region, that does not exhibit high error levels. The white regions within the BT plots indicate those domain points deemed cloudy for this channel by the LCCDR algorithm and thus have been removed from consideration.

The overall structure of the simulated BT field is in good agreement with the observations as well as the magnitude of the temperatures. Since this channel is most sensitive to MM5 temperature, it is reasonable to assume that the MM5 temperature profile (around the 330-hPa level) is in good agreement with the actual temperature profile for T1. In fact, the error for this channel for both T1 and T2 is smaller than 1.0 K. It can be shown that all carbon dioxide channels with peak RS- T within the 300–500-hPa region exhibit similar

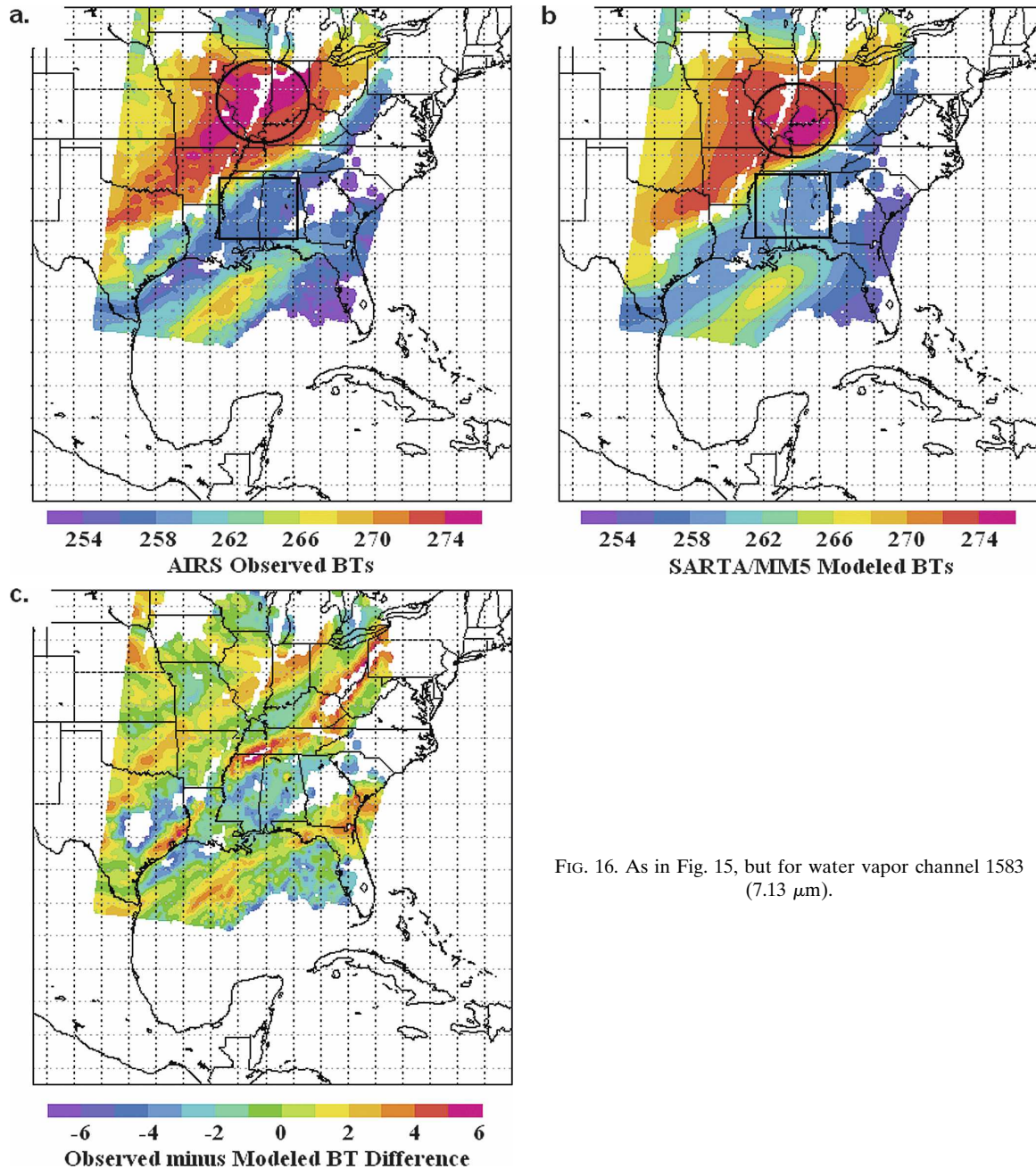


FIG. 16. As in Fig. 15, but for water vapor channel 1583 ($7.13 \mu\text{m}$).

RMS error distributions as that of channel 209 (figures omitted).

Figure 16a shows the spatial BT field for channel 1583 from AIRS and Fig. 16b the MM5/SARTA for T1. This channel is a water vapor channel most sensitive to water vapor and temperature near 600 hPa. The simulated BT field does well at capturing the large-scale pattern of the AIRS observations but not so well in estimating the exact position and extent of the moisture gradient associated with the cold front and the cross-

frontal gradient features. The midlevel moisture gradient associated with a cold front is visible in this channel as a sharp BT gradient cutting across the eastern United States from western Pennsylvania to central Texas. This gradient is visible in this channel because of the effects of water vapor on atmospheric radiance. The greater amount of water vapor in this region leads to a greater absorption and a smaller transmission and thus lower BT values. There appears to be some disagreement between the simulated BTs and the observations

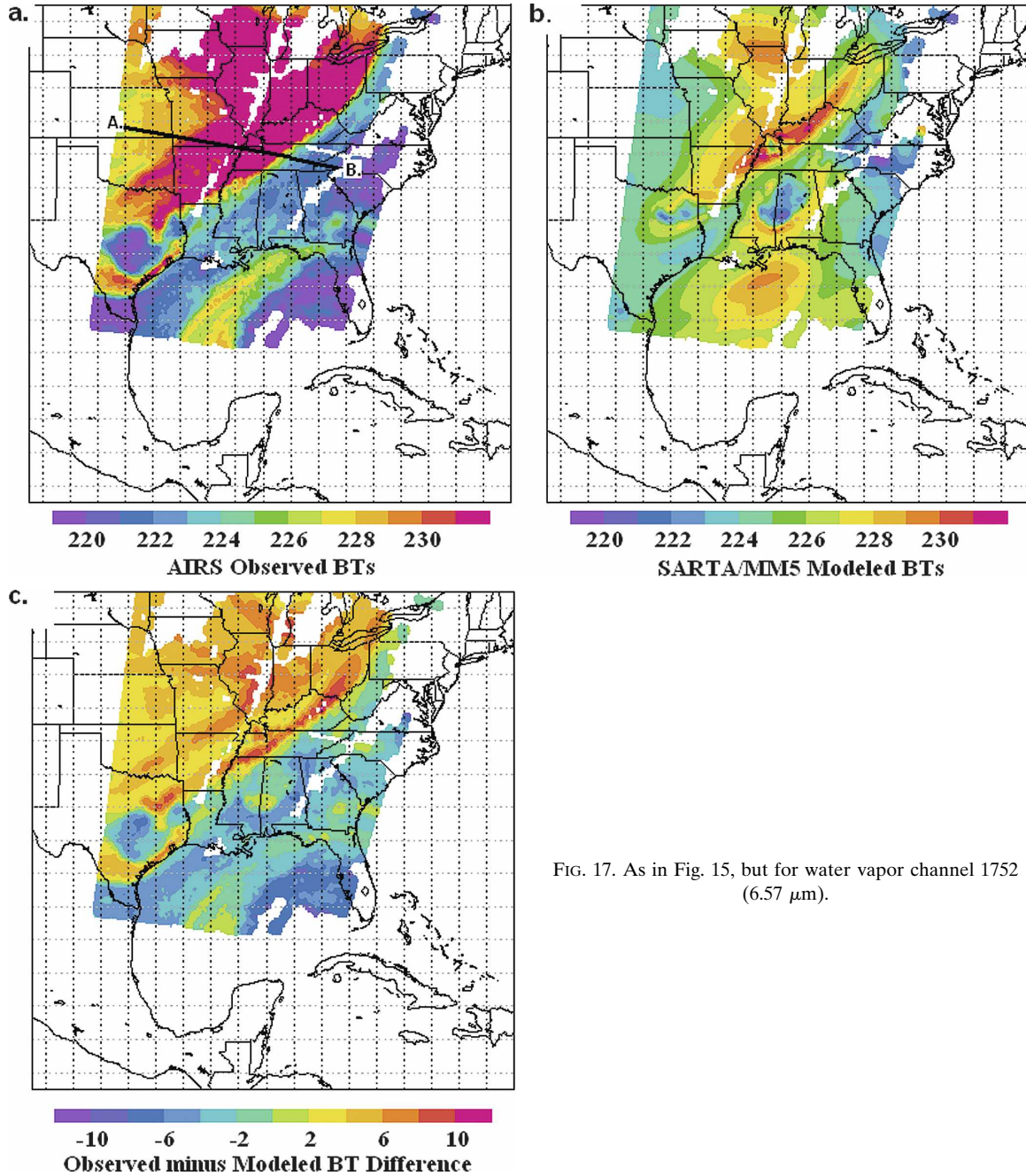


FIG. 17. As in Fig. 15, but for water vapor channel 1752 (6.57 μm).

regarding the magnitude of the atmospheric drying (indicated by the warmer BTs) and the moisture ahead of the front (indicated by the cooler BTs over the eastern United States). The simulated BTs are cooler behind the cold front near the state of Illinois (circled in black) than in the observations; conversely, the simulated BTs are warmer ahead of the cold front over Alabama and Mississippi (boxed in black) than in the observations. This suggests that the MM5 predicted a weaker middle-

level moisture gradient, too-moist conditions behind the gradient, and too-dry conditions ahead.

Figure 17 shows the spatial BT field for another water vapor channel (channel 1752) with the maximum sensitivity located near 310 hPa. This channel is an example of one of the upper-level water vapor channels that exhibit large RMS errors as shown in Fig. 11b. As can be seen here, the simulated BT field barely captures the observed horizontal structure and not at all the

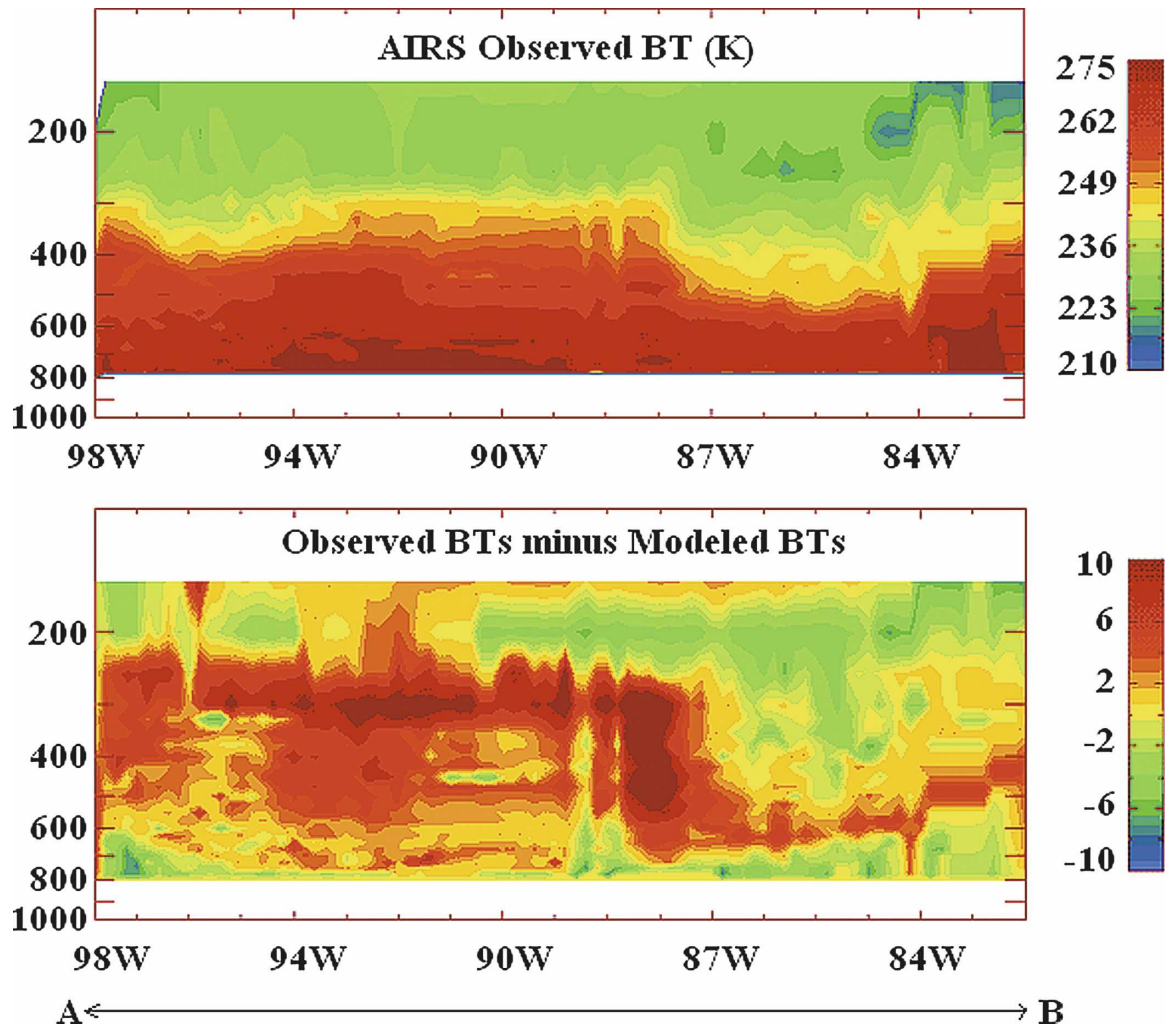


FIG. 18. The BT cross section (A–B line shown in Fig. 17a) with each water vapor channel arranged vertically by peak RS- Q pressure level: (a) AIRS-observed BT data from T1 (granule 078 at 0747 UTC 11 Jul 2003) and panel (b) differences between AIRS-observed and MM5/SARTA-simulated BTs (observation – model simulation).

magnitude. The simulated BT field does capture a gradient-like feature (warmer BTs across the Ohio River valley, with slightly colder temperatures toward the Atlantic seaboard), but the BT difference across the gradient is much smaller than those seen in the observations. It appears that the simulated BT field is the result of the MM5 seriously underpredicting the strength of the moisture gradient at the upper levels, suggesting that the forecast model may be trying to keep the moisture gradient primarily as a midlevel event, and the AIRS observations indicate a much deeper event—a middle- and upper-level event.

To verify the above statement, the vertical structure of the moisture gradient is examined in BT space using the RTM simulation and the AIRS observations. Figure 18 compares the vertical structure of the moisture

gradient along a line cutting across the cold front (see Fig. 17a). Figure 18a shows the AIRS-observed BTs whereas Fig. 18b shows the differences between AIRS-observed and model-simulated BTs. All water vapor channels from the AIRS spectrum are used and have been arranged by their corresponding peak RS- Q pressure level at each point. Red-shaded regions indicate warm BTs, whereas green-shaded regions indicate cooler BTs. Warmer BTs are indicative of more transmission and therefore drier air, while cooler BTs represent less transmission and therefore more moisture. Between 87° and 98°W (Fig. 18a), the data indicate a deeper layer of warmer BTs than for those regions east of 87°W; this is the BT gradient discussed previously. This feature is not captured by the model forecast properly (Fig. 18b). Also, the depth of the warmer BTs

(>270 K) is deeper in the AIRS observations than in the simulated BT field, with the observed BTs being warmer, especially in the upper troposphere, than the corresponding simulated BTs west of 87°W. This indicates that the MM5 is keeping the upper-level atmosphere too moist, which is consistent with our previous findings. Similar results are obtained when comparing the spatial distributions of the MM5 19-h forecast valid at 1900 UTC 11 July 2003 (T2) with AIRS observations (not shown).

It is emphasized that the proposed approach could be used to infer how well the model-forecasted temperature and/or moisture profiles approximate the observed ones at the model resolution, and at what level(s) the model is doing poorly for which variable(s) based on the fitting of radiances. It cannot be used to determine if the real temperature profile is similar to that from the model based on the fitting of radiances. It is possible that the model does not capture all vertical structures and yet the radiance verification looks good because of the relatively broad sensitivity profiles.

5. Summary and conclusions

An adjoint sensitivity study is conducted for all AIRS channels to obtain the vertical structures of their relative sensitivities. The relative sensitivity ranks the relative importance of changes in the temperature and moisture fields at various vertical levels to the simulated radiance values. In other words, the magnitudes of the relative sensitivity indicate at which level changes in temperature and/or moisture will have the largest influence on the simulated values of BT. On the other hand, the vertical structure of WF indicate at which level the model atmosphere (whose state is defined by temperature and/or moisture) contributes to the emission at the top of the atmosphere most significantly. It is shown that the level of the peak RS-*T* value for a given channel could be above or below the maximum WF height. This vertical shift is primarily controlled by the vertical atmospheric temperature structure and the broadness of the WFs. If the peak WF is within a region where the temperature is increasing (decreasing) with height, the corresponding RS-*T* profile will be shifted above (below) the WF profile. The amount of shift is controlled by the broadness of the WF profile in the direction of the shift. For example, if the WF profile is broad (narrow) and has multiple (few) pressure levels of WF > 0.9 in the direction of the shift, the shift will be large (small).

Having illustrated the differences of the vertical structures of sensitivity and WF, the sensitivity results are chosen as a useful input for a forecast verification

using AIRS observations. It has been shown that useful conclusions on model performance can be drawn from comparing model forecasts with AIRS radiances under the guidance of adjoint sensitivity. Through a case study, we are able to show that the MM5 does a fine job of predicting the atmospheric temperature of a case characterized by a middle- and upper-level moisture gradient except during the daytime near the surface. Nonetheless, the model has greater difficulty with the moisture forecast, especially in the upper levels (<400 hPa).

The above adjoint-based forecast verification method provides one with an excellent tool to utilize indirect satellite observations to infer possible errors in forecast fields. More case studies will be carried out. The error signal of the MM5 forecasts found by such an approach will be used for channel selection, targeted observations, and construction of a background error covariance matrix. These applications are being explored and results will be discussed in future papers.

Acknowledgments. This research is supported partially by the NASA Project 20025157 and partially by the NOAA GOES-R project lead by Space Science and Engineering Center (SSEC) at the Cooperative Institute for Meteorological Satellite Studies (CIMSS), Madison, Wisconsin.

REFERENCES

- Amerault, C., and X. Zou, 2003: Preliminary steps in assimilating SSM/I brightness temperatures in a hurricane prediction scheme. *J. Atmos. Oceanic Technol.*, **20**, 1154–1169.
- Aumann, H. H., and Coauthors, 2003: AIRS/AMSU/HSB on the Aqua mission: Design, science objectives, data products, and processing systems. *IEEE Trans. Geosci. Remote Sens.*, **41**, 253–264.
- Baker, N. L., C. B. Blankenship, W. F. Campbell, S. D. Swadley, T. F. Hogan, and E. H. Barker, 2005: Assimilation of AMSU-A/B radiances with the NRL Atmospheric Variational Data Assimilation System (NAVDAS). *Proc. SPIE*, **5658**, 154–165.
- Blackadar, A. K., 1979: High resolution models of the planetary boundary layer. *Advances in Environmental Science and Engineering*, J. Pfafflin and E. Ziegler, Eds., Vol. 1, No. 1, Gordon and Breach, 50–85.
- Carrier, M. J., X. Zou, and W. Lapenta, 2007: Identifying cloud-uncontaminated AIRS spectra from cloudy FOV based on cloud-top pressure and weighting functions. *Mon. Wea. Rev.*, **135**, 2278–2294.
- Chahine, M. T., H. Aumann, M. Goldberg, L. McMillin, P. Rosenkranz, D. Staelin, L. Strow, and J. Susskind, 2001: AIRS-team retrieval for core products and geophysical parameters: Level 2. Algorithm Theoretical Basis Doc. Version 2.2, JPL D-17006, 198 pp.
- Derber, J. C., and W. S. Wu, 1998: The use of TOVS cloud-cleared radiances in the NCEP SSI analysis system. *Mon. Wea. Rev.*, **126**, 2287–2299.
- Dudhia, J., 1993: A nonhydrostatic version of the Penn State–NCAR Mesoscale Model: Validation tests and simulation of

- an Atlantic cyclone and cold front. *Mon. Wea. Rev.*, **121**, 1493–1513.
- Gelaro, R., R. Buizza, T. N. Palmer, and E. Klinker, 1998: Sensitivity analysis of forecast errors and the construction of optimal perturbations using singular vectors. *J. Atmos. Sci.*, **55**, 1012–1037.
- Grell, G., J. Dudhia, and D. Stauffer, 1995: A description of the fifth-generation Penn State/NCAR Mesoscale Model (MM5). NCAR/TN-398+STR, 117 pp.
- Lanzante, J. R., 1996: Resistant, robust and nonparametric techniques for the analysis of climate data: Theory and examples, including applications to historical radiosonde station data. *Int. J. Climatol.*, **16**, 1197–1226.
- Le Marshall, J., and Coauthors, 2006: Improving global analysis and forecasting with AIRS. *Bull. Amer. Meteor. Soc.*, **87**, 891–894.
- McNally, A. P., P. D. Watts, J. A. Smith, R. Engelen, G. A. Kelly, J. N. Thépaut, and M. Matricardi, 2006: The assimilation of AIRS radiance data at ECMWF. *Quart. J. Roy. Meteor. Soc.*, **132**, 935–957.
- Pagano, T. S., and Coauthors, 2002: On-board calibration techniques and test results for the Atmospheric Infrared Sounder (AIRS). *Proc. SPIE*, **4814**, 243–254.
- Strow, L. L., S. Hannon, S. D. Machado, H. Motteler, and D. Tobin, 2003: An overview of the AIRS radiative transfer model. *IEEE Trans. Geosci. Remote Sens.*, **41**, 303–313.
- Zou, X., A. Barcilon, I. Navon, J. Whitaker, and D. Cacuci, 1993: An adjoint sensitivity study of blocking in a two-layer isentropic model. *Mon. Wea. Rev.*, **121**, 2833–2857.
- Zupanski, M., 1995: An iterative approximation to the sensitivity in calculus of variations. *Mon. Wea. Rev.*, **123**, 3590–3604.